




Intermittent swimming of two self-propelled flapping plates in tandem configuration ^{EP}

Cite as: Phys. Fluids **34**, 011905 (2022); <https://doi.org/10.1063/5.0078829>

Submitted: 16 November 2021 • Accepted: 22 December 2021 • Published Online: 10 January 2022

 Linlin Kang (康林林),  Xi-Yun Lu (陆夕云) and  Weicheng Cui (崔维成)

COLLECTIONS

 This paper was selected as an Editor's Pick



View Online



Export Citation



CrossMark

ARTICLES YOU MAY BE INTERESTED IN

[Hydrodynamic performance of an unconstrained flapping swimmer with flexible fin: A numerical study](#)

Physics of Fluids **34**, 011901 (2022); <https://doi.org/10.1063/5.0077312>

[Computational investigation of drop behavior and breakup in peristaltic flow](#)

Physics of Fluids **34**, 012111 (2022); <https://doi.org/10.1063/5.0077205>

[A thermoacoustic heat pump driven by acoustic waves in a hypersonic boundary layer](#)

Physics of Fluids **34**, 011703 (2022); <https://doi.org/10.1063/5.0079611>

LEARN MORE

 Author Services

Maximize your publication potential with
English language editing and
translation services



Intermittent swimming of two self-propelled flapping plates in tandem configuration

Cite as: Phys. Fluids **34**, 011905 (2022); doi: [10.1063/5.0078829](https://doi.org/10.1063/5.0078829)

Submitted: 16 November 2021 · Accepted: 22 December 2021 ·

Published Online: 10 January 2022






View Online



Export Citation



CrossMark

Linlin Kang (康林林),¹  Xi-Yun Lu (陆夕云),^{2,a)}  and Weicheng Cui (崔维成)^{1,b)} 

AFFILIATIONS

¹Key Laboratory of Coastal Environment and Resources of Zhejiang Province, School of Engineering, Westlake University, Hangzhou 310024, Zhejiang, China

²Department of Modern Mechanics, University of Science and Technology of China, Hefei 230026, Anhui, China

^{a)}Electronic mail: xlu@ustc.edu.cn

^{b)}Author to whom correspondence should be addressed: cuiweicheng@westlake.edu.cn

ABSTRACT

Intermittent swimming and schooling individually offer the possibility of energy economy for fish. To study the role of the simultaneous use of both behaviors, the intermittent swimming of two self-propelled plates in tandem configuration is investigated numerically. Two intermittent swimming modes, i.e., the multiple-tail beat (MT) mode and the half-tail beat (HT) mode, are considered. For solitary plate swimming intermittently while maintaining fixed bout period, the propulsion velocity and energy consumption decrease monotonically as the duty cycle increases, consistent with the prediction of the reduced-order model. A pair of plates swimming with independent duty cycle can form orderly configurations, without separating or colliding, when their duty cycles are similar. For the MT mode, the asymmetric wake of the leader enhances the drag on the following plate by inducing an additional oncoming flow against it, making the follower harder to follow. For the HT mode, the symmetric wake of the leader reduces the drag on the follower, making it easier to follow. No significant difference was found in the propulsive performance of intermittent swimming between the leading plate in orderly configurations and solitary plate. The results of efficiency indicate that the HT mode is more economical than the MT mode for the follower. Usually, the smaller the equilibrium gap spacing is, the more efficient the follower is. The results of the cost of transport show that the follower achieves better energy economy for higher propulsion velocity. The results provide some insight into the collective intermittent swimming of fish and are helpful for bionic design.

Published under an exclusive license by AIP Publishing. <https://doi.org/10.1063/5.0078829>

I. INTRODUCTION

Fish schooling is a frequently observed fish behavior in nature. About 25% of adult fishes exhibit schooling behavior, whereas approximately 50% of fish species tend to school during their juvenile stage.¹ Reducing the energy expenditure of fish has been suggested as one of several possible advantages to schooling.^{1–3} For example, the maximum duration of the fish swimming in schools is observed to be two to six times longer than that of solitary fish.⁴ In general, the decrease in tail beat frequency can be considered as a decrease in energy consumption. It was observed that the tail beat frequency of Pacific mackerel in a school is lower than that of a solitary swimming fish,⁵ and the tail beat frequency of the fish swimming at the rear of the school is smaller compared with the fish at the front of the school.⁶ In such collective swimming, individuals are oriented in the same direction, maintain a certain distance from each other, and exhibit coordinated and correlated swimming.^{7,8}

Another interesting feature of the collective behavior of fishes is that they are self-organized and self-emergent due to flow-mediated interactions. Weihs² proposed a hydrodynamic model that reduces a fivefold energy expenditure by steadily swimming in a lattice-like configuration. Lighthill⁹ further conjectured that such stable configurations can be formed spontaneously due to the hydrodynamic effect, without the need for active control mechanisms or collective decision-making. However, Weihs' prediction² and Lighthill's conjecture⁹ are hardly observed in nature.^{3,10} Considering some constraints in the experimental observation of living animals in terms of operability and measurability, a proven strategy for studying the hydrodynamic interactions of animal swimming is to use actively flapping foils/plates as analogues of fish/fins. Because this approach allows for precise measurement and control of motions and hydrodynamic characteristics, there have been a great deal of studies that use systems of actuated foils/plates to study the biologically inspired flow interactions

experimentally and numerically. The foils/plates could either be fixed within an oncoming flow^{11–14} or self-propelled through a flow.^{15–22} Through these works, we can get some general ideas. For example, the orderly formations of multiple self-propelled flapping plates/foils can be spontaneously achieved via flow-mediated interactions,^{15–17} which confirms Lighthill's conjecture. Due to the spatial periodicity of the reversed vortex street shed by the leader, the follower usually has multiple stable following positions. Moreover, the propulsive performance of the follower can be significantly improved in the stable configuration compared with that of solitary swimmers with the same flapping kinematics.¹⁵

To date, these experimental/numerical studies, using multiple self-propelled flapping foils/plates to simulate fish schooling have all assumed that the bodies are actuated by continuous, sinusoidal flapping motions. In general, however, fish do not swim continuously. Many fish species swim intermittently using a burst-and-coast (B&C) strategy,²³ such as northern anchovy,²⁴ golden shiner,²⁵ koi carps,²⁶ cod,^{27,28} saithe,²⁷ zebrafish,^{29,30} *Hemigrammus bleheri*,^{31,32} and Pacific bluefin tuna.³³ The B&C swimming, also called intermittent locomotion, is characterized by a two-phase periodic behavior of alternating accelerations (burst phase) with glides (coast phase).

Energy economy has also been considered the main reason that fish adopt a B&C swimming strategy.^{26,27,34–36} Lighthill³⁶ originally proposed that the B&C swimming can reduce skin friction drag during coast phase and save fish energy by taking advantage of the viscous Bone–Lighthill boundary layer thinning mechanism. Weihs³⁴ further showed that intermittent swimming can reduce energy expenditure by 50% compared with continuous swimming with the same average speed. His model was tested by Videler and Weihs,²⁷ and the results showed that the experimental values for cod and saithe remarkably agree with the model's prediction. Wu *et al.*²⁶ suggested that nearly 45% of energy is saved when B&C swimming is used by the koi carps compared with continuous swimming with the same average speed. Recently, Akoz and Moored³⁷ showed that, in addition to a viscous mechanism,³⁶ there is also an inviscid Garrick mechanism that accounts for most of the observed energy savings by using a B&C swimming strategy. Akoz *et al.*³⁸ further studied intermittent unsteady propulsion with a combined heaving and pitching foil, and discovered that pitch-dominated motions and heave-dominated motions are driven by added mass-based mechanism and circulatory-based mechanism, respectively.

In some recent numerical and experimental works of bio-inspired propulsors,^{39–41} it is confirmed that the intermittent style enjoys some advantages in regard to energy efficiency over the continuous one. However, there are also some disagreements regarding the energy efficiencies. In the inviscid numerical simulations of an intermittently pitching hydrofoil, it was discovered that continuous swimming can actually be more economical when the Reynolds number or the duty cycle is sufficiently low.³⁷ Dai *et al.*⁴² also indicated that intermittent locomotion is more economical than the continuous style only when the Reynolds number is sufficiently large and the duty cycle is moderate. Liu *et al.*⁴³ found that intermittent swimming of flexible plate shows better performance when the bending stiffness is moderate and the duty cycle is not too small. Gupta *et al.*⁴⁴ showed that intermittent swimming is effective for pitching swimming kinematics but not for undulation swimming kinematics. Ashraf *et al.*⁴⁵ further addressed that intermittent swimming is not always energetically

beneficial to fish, which suggests that the primary purpose of intermittent swimming may not be to conserve energy alone, but a combination of other functional aspects such as improved sensing and the likely existence of a minimum tail beat frequency. For example, Bone *et al.*⁴⁶ found that for prolonged swimming at high speeds, the B&C swimming mode is necessary, because the bulk of fast white anaerobic musculature can be exhausted within a few minutes when contracting at full rate.

By measuring the body kinematics of a B&C swimming koi carp, Wu *et al.*²⁶ identified two typical burst modes of koi carp, i.e., multiple-tail beat (MT) mode and half-tail beat (HT) mode. The two modes were also observed by Ashraf,⁴⁷ which appear in low-speed swimming and high-speed swimming, respectively. The simplified numerical/experimental models of intermittent locomotion have assumed that the driving motion of the flapping foils/plates adopts the MT mode and/or the HT mode.^{37,39–42,45}

In addition, the wake structures in intermittent swimming were found to be very different from that behind a continuous swimmer. Moreover, due to dissimilarities in the kinematic parameters—the Reynolds number and the body shape—the wake vortex structures of intermittent swimmers are also different from case to case.^{26,37,39–42} The wake vortex morphology is unlike a continuous undulating vortex pair. It should be noted that the emergent of orderly configurations of fish schooling is closely related to the periodic wake vortices shed by the leading fish. For example, Liao showed that the tail beat frequency of the rainbow trout matches the vortex shedding frequency of the Kármán vortex street.⁴⁸ Since the wake vortical structures of intermittent swimming are different from that of continuous swimming, it indicates that the hydrodynamic mechanism behind intermittent schooling may be more complex than continuous schooling. However, there are no extensive studies on intermittent schooling in terms of hydrodynamics.

There have been very few studies on the simultaneous behaviors of B&C swimming and schooling,^{25,47} and all of them focus on experimental observations of real fish. Ashraf⁴⁷ showed that the average bout period T_{Cyc} , that is, the duration of a burst event (T_B) and its successive coast event (T_C), remains relatively constant over the range of velocities tested. Fish *et al.*²⁵ also observed that, when fish swim intermittently in formation, despite the longer coast time observed for trailing fish compared with leading fish, no significant differences were detected for the total time T_{Cyc} of the B&C cycle between fish. The results also indicate that energy economy through the use of intermittent swimming behavior can be enhanced by swimming in formation, particularly for trailing fish. Although intermittent locomotion can reduce the cost of locomotion at the individual level, the link between the optimization of individual intermittent locomotion and the collective behavior, especially among members with different duty cycle, is unknown.

As a natural extension of previous works, the intermittent swimming performance of collective self-propelled flapping plates in tandem configuration is investigated in this paper. The purpose of this study was to investigate the interaction of schooling and intermittent swimming style for possible stable configuration and hydrodynamic advantages. Considering that fish groups involve variation of fin motions, the flapping kinematics of each plate are independently prescribed and systematically varied, while the forward swimming motions are free and result from fluid–structure interaction. To our

knowledge, no such studies have been published. The propulsive performance is compared between solitary plates and a pair of plates in tandem configuration.

The rest of this paper is arranged as follows. The physical problem, governing equations, and numerical methods are described in Sec. II. The results and discussions regarding the propulsive performance (orderly configurations, swimming speeds, energy cost, efficiency, etc.) of the intermittent collective locomotion of two self-propelled flapping plates in tandem configuration and the wake structures are discussed in Sec. III. The concluding remarks are addressed in Sec. IV. Finally, the nomenclature, a detailed introduction of the numerical methodology, and the derivation of the simplified dynamical model are presented in Appendixes A and B.

II. PROBLEM DESCRIPTION AND NUMERICAL METHOD

A. Physical problem and mathematical formulation

A computational study is performed to study the collective dynamic and propulsion performance of two self-propelled plates flapping intermittently in tandem configuration. The nomenclature of all key quantities involved in this paper is presented. As shown in Fig. 1(a), the fish-like swimmer is modeled as an elastic plate driven at the leading edge by the heaving motions. The plates are allowed to move freely in the direction aligned with the x axis, as a result of fluid-structure interactions. The prescribed heaving motions at the leading edge of the plates are described in Fig. 1(b). The multiple-tail beating (MT) mode and half-tail beating (HT) mode are assumed here for the actuation of intermittent swimming. The degree of intermittent locomotion is captured in the duty cycle ($DC = T_b/T_{cyc}$ for the MT mode, $DC = 2T_b/T_{cyc}$ for the HT mode), which is the ratio of the burst phase to the total flapping cycle T_{cyc} . T_c is the interval of the coast phase.

Since there is no significant difference in the time duration of one full B&C cycle between fish in orderly formation,^{25,47} the total flapping period T_{cyc} is the same for the two plates. The flapping amplitude A is also a fixed parameter, since in the cruising state, the tail beating amplitude is a constant proportion of the length at all speeds while the tail beat frequency changes with speed.⁴⁹ In addition, in the present

work, we do not consider phase shift between the two plates, because the phase shift for the flapping motion does not affect the interaction between the follower and the wake left by the leader.^{15,21}

For the B&C swimming of the MT mode, a certain time duration of passive coasting is interspersed after completing one period of active bursting. The kinematics for the MT mode can be written as follows:

$$y_{head} = \begin{cases} A \cdot \cos\left(\frac{2\pi(ft - \lfloor ft \rfloor)}{DC}\right), & ft - \lfloor ft \rfloor \leq DC, \\ A, & DC < ft - \lfloor ft \rfloor \leq 1, \end{cases} \quad (1)$$

where $\lfloor \cdot \rfloor$ is the symbol for rounded down, y_{head} is the lateral position of the leading edge, A is the heaving amplitude, and $f = 1/T_{cyc}$ is the flapping frequency for the full cycle.

In the HT mode, certain time durations of passive coasting are interspersed between two half-periods of active bursting. The prescribed heaving motion at the leading edge is described as follows:

$$y_{head} = \begin{cases} A \cdot \cos\left(\frac{2\pi(ft - \lfloor ft \rfloor)}{DC}\right), & ft - \lfloor ft \rfloor \leq DC/2, \\ -A, & DC/2 < (ft - \lfloor ft \rfloor) \leq 0.5, \\ -A \cdot \cos\left(\frac{2\pi(ft - \lfloor ft \rfloor - 0.5)}{DC}\right), & 0.5 < (ft - \lfloor ft \rfloor) \leq 0.5 + DC/2, \\ A, & 0.5 + DC/2 < (ft - \lfloor ft \rfloor) \leq 1. \end{cases} \quad (2)$$

Since, for the HT mode $T_{cyc} = 2(T_b + T_c)$. If $T_b = T_{cyc}/2$, the intermittent motion becomes continuous motion.

The motion of the fluid is governed by the incompressible Navier–Stokes equations given by

$$\frac{\partial \mathbf{u}}{\partial t} + \mathbf{u} \cdot \nabla \mathbf{u} = -\frac{1}{\rho} \nabla p + \frac{\mu}{\rho} \nabla^2 \mathbf{u} + \mathbf{f}, \quad (3)$$

$$\nabla \cdot \mathbf{u} = 0, \quad (4)$$

where \mathbf{u} is the velocity, p the pressure, ρ the density of fluid, and μ the dynamic viscosity. \mathbf{f} is the Eulerian force acting on the surrounding

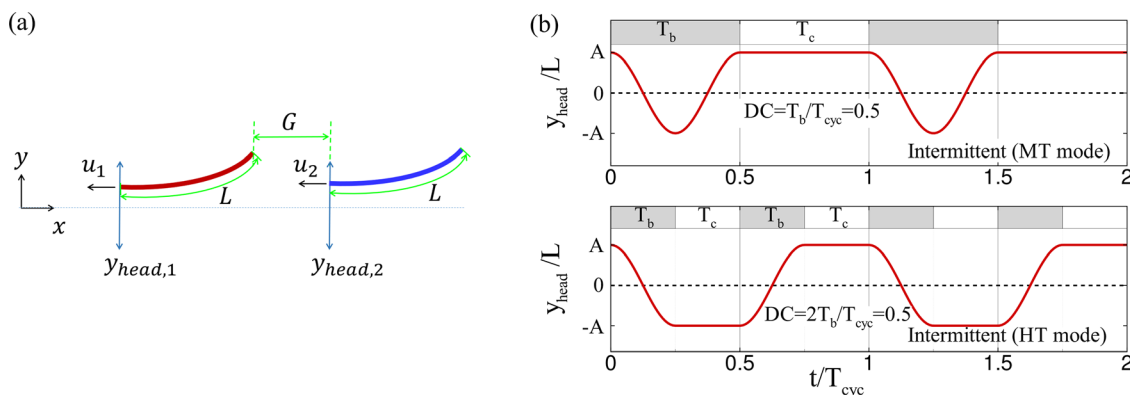


FIG. 1. (a) Schematic diagram for the two self-propelled plates driven by plunging motions in tandem configuration. $y_{head,i}$ and u_i are the lateral coordination and propulsion velocity of the i th plate, respectively. L is the length of each plate. G is the gap spacing between the two plates. (b) Kinematics of the head of the plates for intermittent swimming (in the MT mode and the HT mode) with $DC = 0.5$. T_b and T_c are the time durations for the active and passive phases of B&C swimming, respectively. $T_{cyc} = T_b + T_c$ for MT mode, $T_{cyc} = 2(T_b + T_c)$ for the HT mode.

fluid due to the immersed boundary (IB), as constrained by the velocity boundary condition.

The motion of the elastic plate is governed by the nonlinear partial differential equation⁵⁰

$$\rho_s h \frac{\partial^2 \mathbf{X}}{\partial t^2} - \frac{\partial}{\partial s} \left[Eh \left(1 - \left| \frac{\partial \mathbf{X}}{\partial s} \right|^{-1} \right) \frac{\partial \mathbf{X}}{\partial s} \right] + EI \frac{\partial^4 \mathbf{X}}{\partial s^4} = \mathbf{F}_s, \quad (5)$$

where s is the Lagrangian coordinate along the plate, \mathbf{X} is the position vector of the plate, $\rho_s h$ is the structural linear mass density, Eh and EI are the structural stretching rigidity and bending rigidity, respectively. \mathbf{F}_s is the Lagrangian force exerted on the plates by the surrounding fluid.

In addition to satisfying the prescribed governing equation (1) or (2), the leading edge of the plate satisfies boundary conditions $\frac{\partial \mathbf{X}}{\partial s} = \mathbf{e}_x$ and $-Eh \left(1 - \left| \frac{\partial \mathbf{X}}{\partial s} \right|^{-1} \right) \frac{\partial \mathbf{X}}{\partial s} + EI \frac{\partial^3 \mathbf{X}}{\partial s^3} = \mathbf{0}$, where \mathbf{e}_x is the unit vector in the x direction. The conditions $-Eh \left(1 - \left| \frac{\partial \mathbf{X}}{\partial s} \right|^{-1} \right) \frac{\partial \mathbf{X}}{\partial s} + EI \frac{\partial^3 \mathbf{X}}{\partial s^3} = \mathbf{0}$ and $\frac{\partial^2 \mathbf{X}}{\partial s^2} = \mathbf{0}$ are imposed at the trailing edge.

We choose the reference quantities L , ρ , and U_{ref} to nondimensionalize the above mathematical formulation, where U_{ref} is the reference velocity (defined as $U_{ref} = Lf$). The dimensionless parameters are defined as follows: the heaving amplitude is A/L , the Reynolds number $Re = \rho U_{ref} L / \mu$, the bending stiffness $K = EI / \rho U_{ref}^2 L^3$, the stretching stiffness $S = Eh / \rho U_{ref}^2 L$, the mass ratio of the plates $M = \rho_s h / \rho L$, and the gap spacing G/L . In the following descriptions, A and G denote the normalized quantity A/L and G/L .

B. Numerical method and validation

The Navier–Stokes equations are solved numerically by the lattice Boltzmann method (LBM).^{51,52} The deformation and motion of flexible plates are described by a structural equation, which is solved by a finite element method⁵³ in the Lagrange coordinate independently. For each plate, boundary conditions for the leading and trailing ends are imposed. The movement of each plate (Lagrange points) is coupled with the LBM solver through the immersed boundary (IB) method. The body force \mathbf{f} in Eq. (3) represents an interaction force between the fluid and the immersed boundary to enforce the no-slip velocity boundary condition, which on the Eulerian points can be obtained

from the Lagrangian force \mathbf{F}_s using the Dirac δ function.⁵⁴ See Appendix A for a detailed description of the numerical method.

Based on our convergence studies with different computational domains, the computational domain is chosen as $50L \times 30L$ in the x and y direction. The mesh is uniform with spacing $\Delta x = \Delta y = 0.01L$. The time step is $\Delta t / T_{cyc} = 1/10\,000$ with T_{cyc} being the full flapping period. Such grid spacing and time step can ensure that the Mach number is sufficiently low to reduce deleterious compressibility effects affecting the solution of the lattice Boltzmann equation (LBE). A finite moving computational domain is used in the x direction. As the plate travels one mesh spacing in the horizontal direction, the computational domain is shifted by adding one layer at the inlet and removing one layer at the outlet.⁵⁵

To study grid independence and time step independence, the elastic plate swimming intermittently with the MT mode ($DC = 0.5$) is simulated. The propulsion velocity and input work of the plate in simulations with different mesh sizes and time step sizes are shown in Fig. 2. It is seen that $\Delta x/L = 0.01$ and $\Delta t/T_{cyc} = 0.0001$ are sufficient to achieve accurate results.

In addition, the above numerical strategy has been successfully applied to a wide range of fluid–structure interaction problems, such as flow over a circular flexible plate⁵⁶ or an inversed flexible plate,⁵⁷ continuous locomotion of one or more flexible flapping plates,^{17,21,55,58} and intermittent locomotion of a self-propelled flapping plate.⁴³ A similar numerical strategy was also independently developed by De Rosi *et al.*^{59,60} and was also successfully used to study the aeroelastic problem of flexible flapping wings.⁶¹

III. RESULTS AND DISCUSSION

The dimensionless parameters in the present work are shown in Table I. Here, the plate is assumed to be inextensible with a large stretching coefficient $S = 1000$. The mass ratio is chosen as $M = 0.2$, since the inertial force of the structure for flexible fins is smaller than the fluid dynamic loading. Kim *et al.*⁶² indicates that the inertial force of the structure does not influence the cruising speed significantly for $M \leq 1$. The bending stiffness $K = 30$ corresponds to high propulsive efficiencies,⁵⁵ which also belongs to the bending stiffness of real fins, i.e., $K \approx 25 - 230$ for the tail fin of a goldfish. The Reynolds number is fixed as $Re = 200$, which belongs to the range of intermittent swimming of some fish. For example, Larval northern anchovy

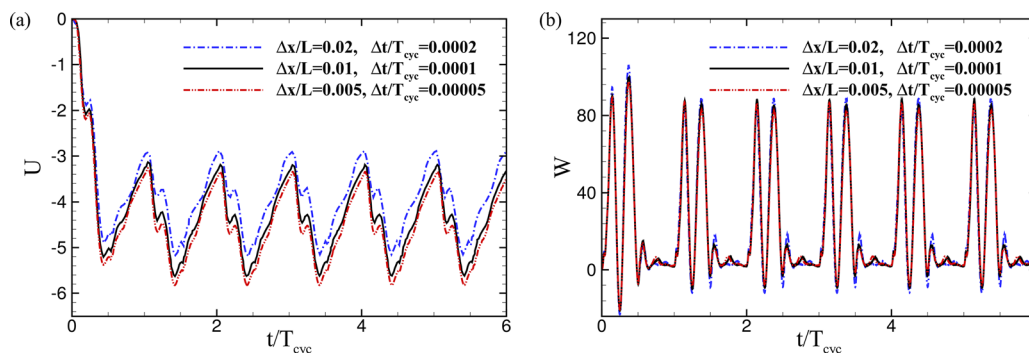


FIG. 2. The grid independence and time step independence studies for the MT mode with $DC = 0.5$, $Re = 200$, $A = 0.2$, $M = 0.2$, $K = 30$, $S = 1000$. The time evolution of (a) the propulsion velocity U and (b) the input work W done on the fluid.

TABLE I. Key parameters in the simulations.

Reynolds number, Re	200
Heaving amplitude, A	0.2
Mass ratio, M	0.2
Stretching stiffness, S	1000
Bending stiffness, K	30
Duty cycle, DC	0.2, 0.3, 0.4, 0.5, 0.6, 0.7, 0.8, 0.9, 1.0

begin to swim intermittently when their typical Reynolds number reaches $Re \approx 100$.^{29,33}

A. Performance of solitary intermittent flapping plate

The aim of this subsection is to give some intuitive understanding of the propulsive performance and flow field characteristics of solitary flapping plates swimming intermittently. First, as shown in Fig. 3, the intermittent swimming of a solitary flexible plate with $DC=0.5$ is taken as an example to analyze the deformation, propulsive velocity, and the input work of flexible plates in a full cycle of B&C swimming. It is seen that the deformation, the propulsion velocity increase, and the energy consumption mainly occur in the burst stage (solid line in Fig. 3). In contrast, in the coast stage (dashed line), the deformation gradually recovers, the propulsion velocity decreases monotonously, and there is almost no energy consumption. In addition, in the burst stage, the increase in deformation and energy consumption mainly occurs in the flapping acceleration stage.

To analyze the effect of duty cycle on the propulsive performance of intermittent swimming, the mean propulsion velocity U_c , the mean input work \bar{W} , the propulsive efficiency η , and the cost of transport (COT) are introduced. The definitions of the above quantities are as follows:

$$U_c = -\frac{1}{T_{cyc}} \int_{t'}^{t'+T_{cyc}} \left(\frac{\partial X}{\partial t} \right)_{s=0} dt, \tag{6}$$

$$\bar{W} = \int_{t'}^{t'+T_{cyc}} a(t) \left[\int_0^1 F \cdot \frac{\partial \mathbf{X}}{\partial t} ds \right] dt, \tag{7}$$

where F represents the force on the surrounding fluid by the plate, and the shielding function $a(t)$ is defined as

$$a(t) = \begin{cases} 0, & t \in \text{coast interval,} \\ 1, & t \in \text{burst interval.} \end{cases} \tag{8}$$

The propulsive efficiency η is the ratio of the kinetic energy of the plate and the input work, i.e.,

$$\eta = \frac{1}{2} m U_c^2 / \bar{W}. \tag{9}$$

The cost of transport (COT) of a swimming fish is defined as the metabolic energy required to transport a unit mass a unit distance. Its dimensionless form is defined as follows:

$$COT = \frac{\bar{W}}{M U_c T_{cyc}}. \tag{10}$$

Figure 4 shows the average propulsion velocity U_c and input work \bar{W} as a function of the duty cycle of intermittent swimming. For both the MT mode and the HT mode, the average propulsion velocity U_c and input work \bar{W} decrease monotonically with increase in DC . No significant difference was found between the MT mode and the HT mode. It should be noted that the change of U_c with DC is different from the previous results.^{42,43} This is because, in these works the duration of the burst phase T_b is fixed when DC changes, while in the present work, the full flapping period T_{cyc} is fixed when DC changes. To explain the above results, in Appendix B, a simplified dynamic model is introduced to predict the relation between the duty cycle DC and the propulsive performance. By assuming $|u - U_c| \ll |U_c|$ for fixed T_{cyc} , we can get a reduced-order relationship, i.e., $U_c \sim \beta / \sqrt{DC + 2DC^2}$ and $\bar{W} = \gamma / (DC\sqrt{DC + 2DC^2})$, where β and γ are constant coefficients. The reduced-order relations are denoted by a solid line in Fig. 4. The $DC - U_c$ and $DC - \bar{W}$ relationships predicted by the model show the same monotonicity as the numerical results.

Figure 5 shows the swimming efficiency (η) and the cost of transport (COT) of a solitary plate swimming intermittently with the MT mode and the HT mode, respectively. For the MT mode, the efficiency η increases monotonically with increase in DC , while for the HT mode, the relation ($\eta - DC$) is not monotonic. It is seen that the MT mode is slightly more efficient than the HT mode, except for $DC=0.5$. The highest efficiency occurs at continuous swimming, i.e., $DC=1$. Figure 5(b) shows that the cost of transport (COT) decreases monotonically with increase in DC , and the two modes almost coincide. The lowest cost of transport also occurs at $DC=1$. It is seen from

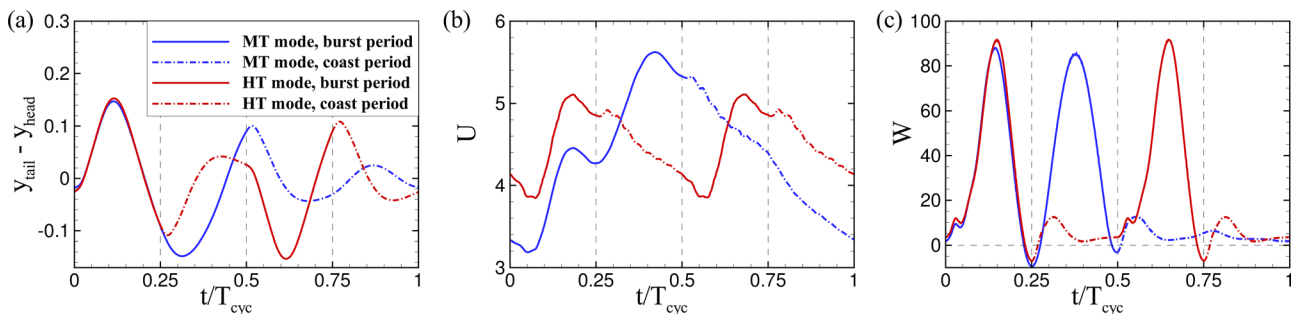


FIG. 3. (a) The lateral displacement of the tail relative to the head ($y_{tail} - y_{head}$), (b) the propulsive velocity U , and (c) the input power W for the MT mode swimming (blue curve) and the HT mode swimming (red curve), respectively. The duty cycle is $DC=0.5$.

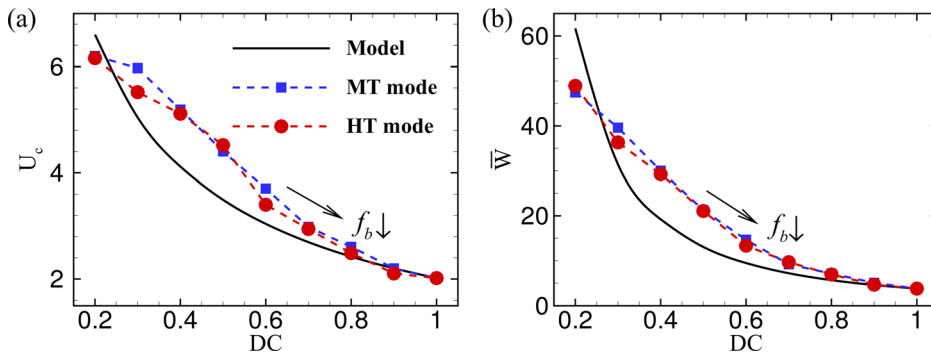


FIG. 4. (a) The average propulsion velocity U_c and (b) the input work W for various duty cycles (DCs) of a solitary plate swimming intermittently. $T_{cyc} = 1$. $f_b = 1/(DC \cdot T_{cyc})$ is the flapping frequency of the burst phase.

Fig. 5(c) that the cost of transport (COT) increases monotonically with increase in the propulsion velocity (U_c), which is consistent with the previous results.^{42,43}

The vortical structures behind the swimmer at various DC values for the MT mode and the HT mode are compared in Fig. 6. For continuous swimming ($DC = 1.0$), one pair of vortices is shed from the tail within a full cycle of flapping, and a reversed Karman vortex street is formed. With decrease in DC, the number of vortices shed from the tail in a full flapping period (T_{cyc}) shows an increasing trend. For intermittent swimming with the MT mode, the vortices shed from the tail are mainly positioned along two lines: the lower vortex street is formed in the burst phase while the upper vortex street is mainly generated in the coast phase. When DC is large, such as $DC = 0.8$, the vortex strength of the upper street is weak due to the shorter coast duration. With an increase in DC, the vortex shedding during the coast phase is strengthened, and the angle between the two vortex streets increases. When DC is small, such as $DC = 0.2$, the characteristic of the two vortex streets disappears, many small vortices shed in the coast stage, and the relative position of strong vortex dipoles generated during the burst phase varies continuously due to vortex induction. For intermittent swimming with the HT mode, the wake vortices can be categorized into three vortex streets. The upper vortex street and lower vortex street consist of strong vortex dipoles formed in the burst phase, while the middle street is made up of wake vortices shed during the coast phase. When DC is large, such as $DC = 0.8$ or 0.6 , the middle street is very weak. Due to mutual induction between the other two

vortex streets, they merge into one vortex street in the far-field wake. For $DC = 0.2$, the vortices generated during the coast stage are mainly rolled into the two vortex streets formed in the burst stage.

Compared with continuous flapping, the wake of the flexible plate with intermittent motion is more complex, which means that the propulsive performance of intermittent collective motion is also more complex than continuous collective motion. In spite of this, we can still find the possible influence of vortical wakes of two different modes (the MT mode and the HT mode) on the follower for a two-plate system in tandem configuration. Take $DC = 0.8$ as an example. As shown in Fig. 6(b), the region between the two dashed lines represents the motion region of the follower with the same flapping amplitude as the leader. According to Biot-Savart formula, the velocity of a point is mainly induced by the vortices near it. Then, we can find from Fig. 6(b) that, for the MT mode, the vortical wake induces a velocity of jet type ($u' > 0$, where u' is the streamwise velocity induced by vortices) for the follower, which may make the follower harder to follow; for the HT mode, the vortical wake induces a velocity of wake type ($u' < 0$) for the follower, which makes the follower easier to follow the leader. The conclusion is also true for other DCs, which is verified by Fig. 7.

As shown in Fig. 7, the time-averaged streamwise velocity field of the MT mode and the HT mode is quite different. For the MT mode, the time-averaged streamwise velocity field can be divided into two layers: the upper layer is of jet type ($\bar{u}' > 0$) and the lower layer is of wake type ($\bar{u}' < 0$). But for the case of $DC = 0.2$, due to the self-induction of the far-field wake vortices [as shown in Fig. 6(e)], the

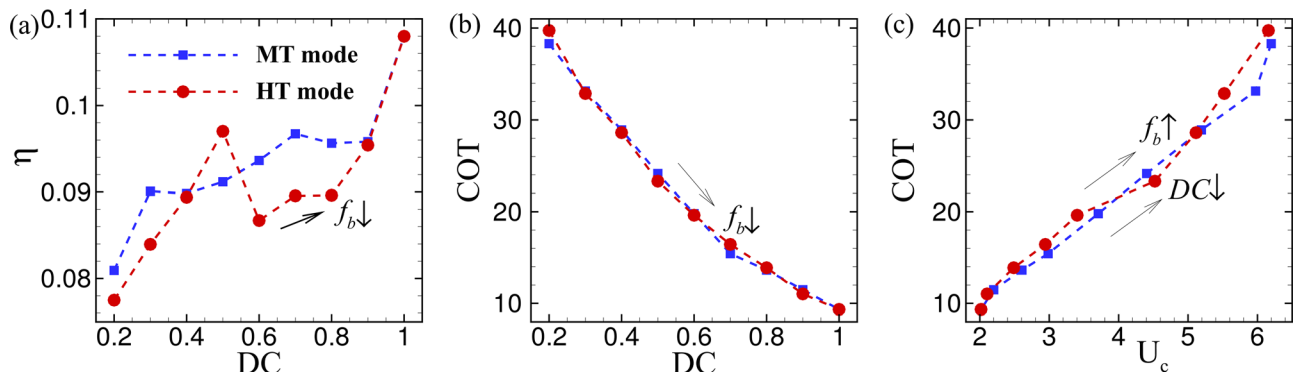


FIG. 5. (a) The swimming efficiency η and (b) the cost of transport COT for various duty cycles (DCs) of a solitary plate swimming intermittently. (c) The cost of transport COT as a function of the propulsion velocity U_c .

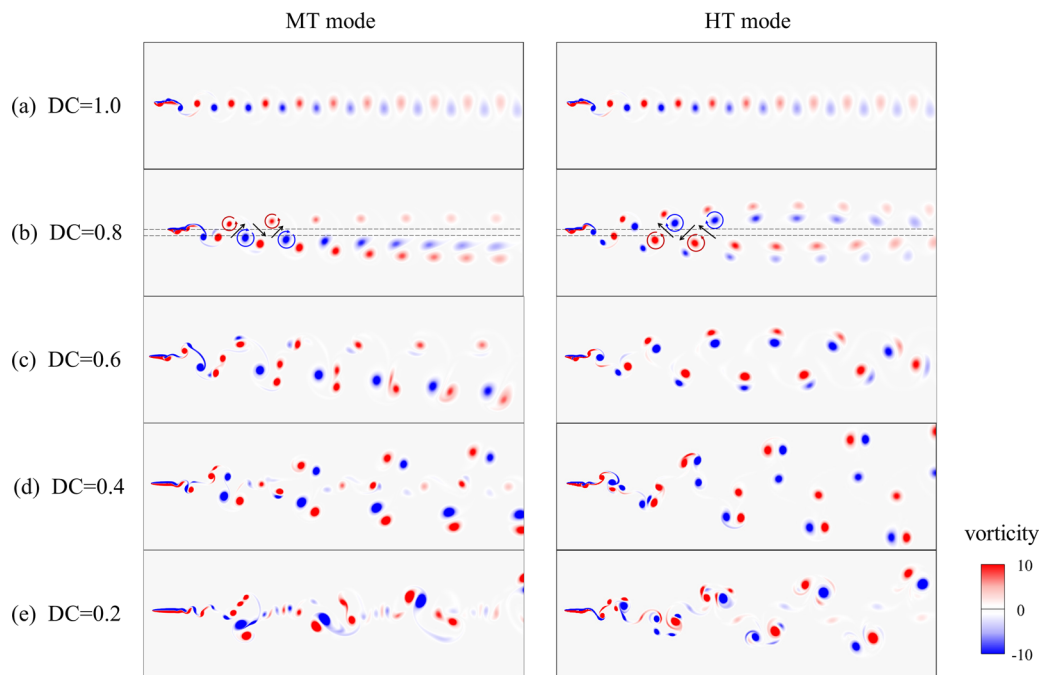


FIG. 6. Instantaneous vorticity contours of the fluid field for B&C swimming of the MT mode (left column) and the HT mode (right column), respectively. The duty cycles corresponding to these vorticity contours are (a) $DC = 1.0$, (b) $DC = 0.8$, (c) $DC = 0.6$, (d) $DC = 0.4$, and (e) $DC = 0.2$, respectively. The contour domain is $24L \times 8L$.

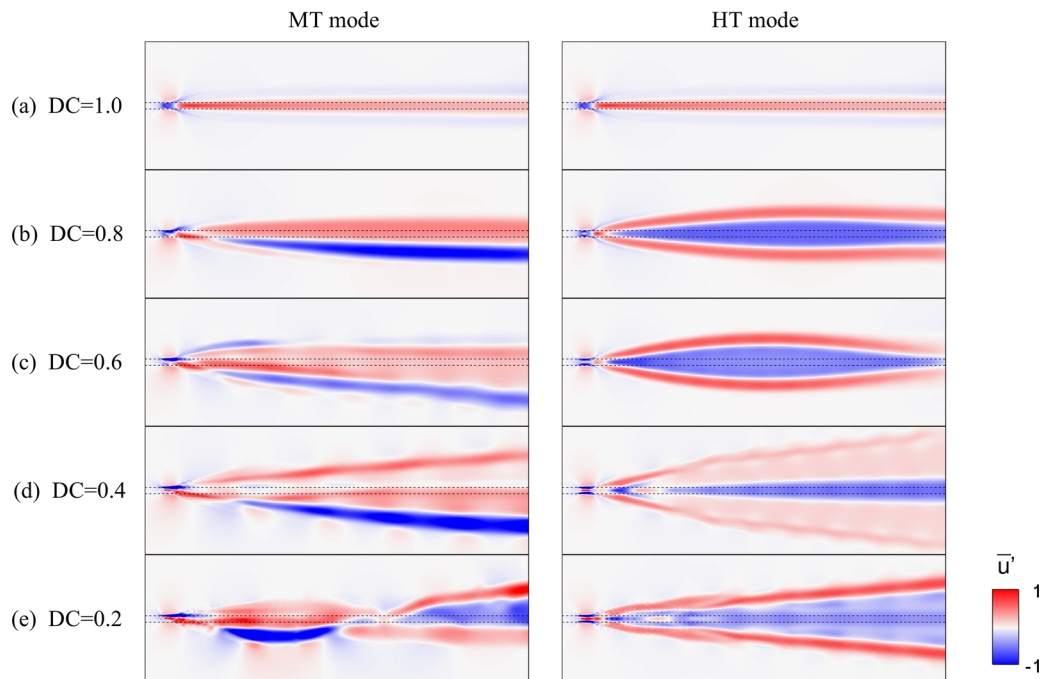


FIG. 7. Time-averaged streamwise velocity field for the MT mode (left column) and HT mode (right column). The duty cycles are (a) $DC = 1.0$, (b) $DC = 0.8$, (c) $DC = 0.6$, (d) $DC = 0.4$, (e) $DC = 0.2$, respectively. The contour domain is $24L \times 8L$.

time-averaged streamwise velocity field becomes a three-layer structure in the far-field wake. For the HT mode, the time-averaged streamwise velocity field can be divided into three layers: the middle layer is of wake type, and the upper and lower layers are of jet type.

B. Performance of a two-plate system in tandem configuration

As mentioned in Sec. I, an interesting feature of collective motion is that multiple individuals spontaneously form stable configurations in which the equivalent gap spacing between individuals is constant. For continuous collective locomotion of flexible plates in tandem configurations, it is found that the follower usually has multiple stable positions in the wake of the leader due to the spatial periodicity of the reversed Karman vortex street,^{15,17} as shown in Fig. 6(a). The equivalent gap spacing [$G_{eq} = \int_{t'}^{t'+T_{cyc}} G(t) dt$] between the two plates is about an integer multiple of the wavelength ($\lambda = U_c T_{cyc}$) of the leader, as shown in the first subfigure of Fig. 8(a). In this subsection, we will investigate whether individuals with different intermittent flapping kinematics can form stable configurations, and the propulsive performance of the pair in stable configurations.

The dynamic configurations of the two plates are categorized in Fig. 8 across the kinematic parameter space of DC_L and DC_F . DC_L and DC_F are the duty cycles of the leader and the follower, respectively. Each point in Figs. 8(b) and 8(c) represents a case that we simulated. As shown in Fig. 8(a), the configurations fall into two main categories: stable orderly configuration with the follower holding a stable position in the wake of the leader (blue curves) and unstable configuration where the gap spacing between the pair will continuously increase (red curves) or decrease (green curves). Figure 4 indicates that when the duty cycles of the leader and follower differ too much, their individual propulsion performances could be very different, they could not form a stable orderly configuration, which is verified by Figs. 8(b) and 8(c). For example, when (DC_L, DC_F) belongs to the red point region, the vortical wake of the leader cannot provide enough constructive momentum for the follower to obtain the same propulsive velocity as the leader, and the following plate is left behind by the leader. Similarly, when (DC_L, DC_F) belongs to the green point region, the

vortical wake of the leader cannot prevent the follower from getting close to the leader and colliding with it. When the two plates have similar propulsive performance ($|DC_F - DC_L| \leq 0.2$), there is at least one stable position for the follower. The results are consistent with the experimental observation of real fish,²⁵ which shows that the trailing fish in the school is different from the leading fish with increased duty cycle by 19%. For the MT mode, the pair with the same duty cycle can form orderly configurations. In contrast, for the HT mode, there are some exceptions, for example the pair with $DC_L = DC_F = 0.3$ or 0.6 cannot form an orderly configuration.

It is known that whether the leader and follower can form orderly configurations depends on the interaction between the follower and the vortical wake shedding from the leading.^{18,21} As shown in Fig. 6, the vortical wake of the plate swimming intermittently is not distributed periodically in space, which indicates that, for intermittent swimming, the stable positions of the follower are not as simple as that for continuous swimming. The initial gap spacing (G_0) of the plates will affect whether the pair can form an orderly configuration and the follower's final equilibrium position. In our simulation, for each given (DC_L, DC_F) , the G_0 value is in the range $[1, \min(5\lambda, 24L)]$, the step is 1, and $\lambda = U_c(DC_L)T_{cyc}$ is the wavelength of the leader. Figure 9 shows the possible equilibrium gap spacings for the combined parameters (DC_L, DC_F) . It is seen that for different (DC_L, DC_F) , the stable positions of the follower are different. The equilibrium gap spacing of the pair depends mainly on the wavelength of the leader, which can approximately denote the spatial characteristics of the leader's vortical wake. In addition, once the orderly configuration is formed, the propulsion velocity depends only on DC_L and is not affected by DC_F . Moreover, for each stable configuration, the propulsion velocity of the pair is the same as that of solitary plate swimming with $DC = DC_L$.

According to a previous simplified mode,^{18,21} the drag on the follower is proportional to the square of the propulsion velocity relative to the ambient fluid, i.e., $D \sim (u_2 - u')^2$. For the follower in orderly configuration, $u_2 \approx -U_c$ is negative. u' is the streamwise velocity in the wake of the leader, of which the time-averaged contour is shown in Fig. 7. By a reduced-order approximation, we can conclude that, if the wake of the leader is of wake type ($u' < 0$), the drag on the

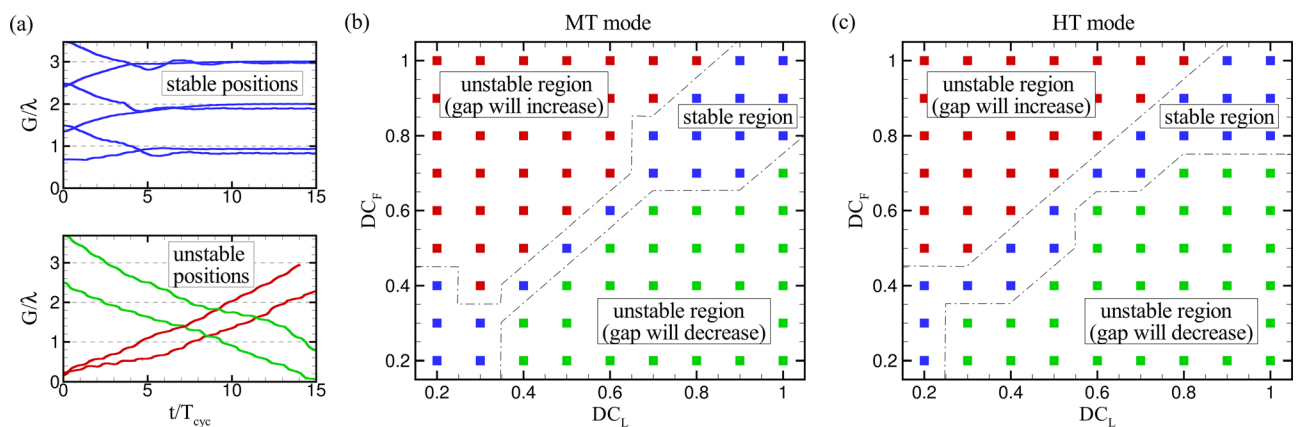


FIG. 8. (a) Sketch for multiple stable positions (blue curve) and unstable positions (red and green curves). [(b) and (c)] Parameter space for two plates swimming independently and intermittently with the MT mode and the HT mode. DC_L and DC_F are the duty cycles of the intermittent swimming of the leading plate and following plate, respectively. The dynamical state of the follower is categorized by color.

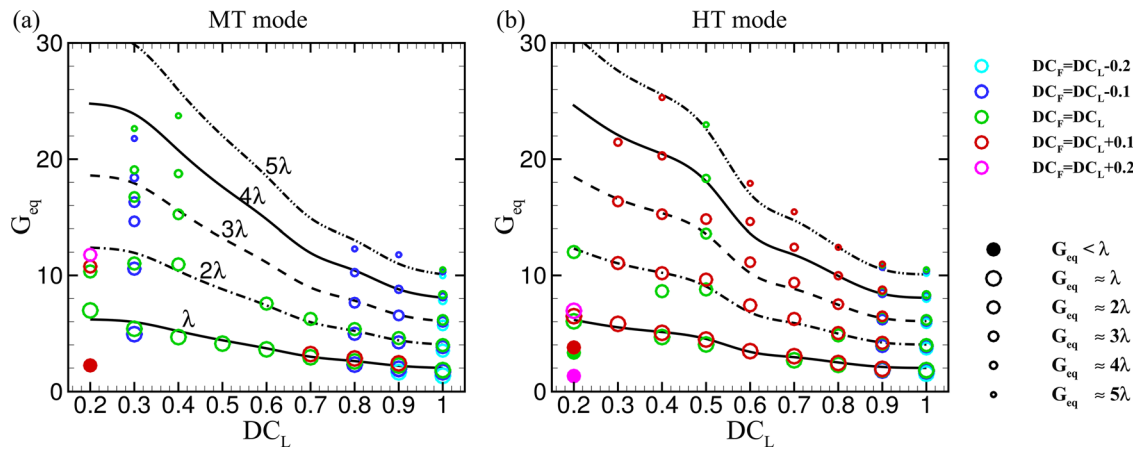


FIG. 9. The equilibrium gap spacing (G_{eq}) as a function of the duty cycle (DC_L) of the leader for (a) the MT mode and (b) the HT mode. $\lambda = U_c(DC_L)T_{cyc}$ is the wavelength of the leader. The color of the points denotes the duty cycle difference ($DC_F - DC_L$) of the follower relative to the leader. The size of the points denotes the relative gap spacing of the follower's stable positions.

following plate will be reduced, whereas if the leader has a jet type wake ($u' > 0$), then the drag on the follower will be enhanced. For the MT mode, when the duty cycle is very small, such as $DC_L = 0.2$, the equilibrium gap spacing is within twice the wavelength, because the far-field wake of the leader [as shown in Fig. 7(e)] reduces the drag on the follower, making it continue to approach the leader until it finds a stable position. In contrast, if the duty cycle is large, such as $DC_L > 0.5$, the wake of the leader changes into jet type as shown in Fig. 7. So, for $DC_F = DC_L$, if the initial gap spacing G_0 is very big, the follower will be left behind, while for $DC_F < DC_L$, there are many stable positions for the follower. For the HT mode, because the wake of the leader is of wake type as shown in Fig. 7, the cases with $DC_F = DC_L + 0.1$ have many stable positions, while for $DC_F = DC_L$, if the initial position of the follower is very far from the leader, it will be sucked to closer stable positions due to reduced drag.

The input works are investigated for those cases with orderly configurations as shown in Fig. 10. For both modes, there is no significant difference in the input work between the leading plate in collective configuration and solitary plate with the same duty cycle. The same phenomenon was also found in continuous collective locomotion of foils/plates^{15,58} and in the intermittent swimming of schooling fish.²⁵ As shown in Figs. 10(b) and 10(c), for the MT mode with $DC_F = DC_L = DC$, the energy consumption of the follower is smaller than the leader when $DC \leq 0.5$ or $DC = 1.0$. For $0.6 \leq DC \leq 0.9$, there are some equilibrium positions for the follower to consume more energy than solitary plate with the same duty. For $DC_F > DC_L$, the energy consumption of the follower is smaller than the leader. For $DC_F < DC_L$, the energy consumption of the follower is greater than the leader, but smaller than a solitary plate with the same duty as the follower. It is shown in Figs. 10(e) and 10(f) that, for the HT mode, the energy consumption of the follower is smaller than that of the leader, and is also smaller than that of the solitary plate with the same duty as the follower [except for $(DC_L, DC_F) = (0.5, 0.6)$ and $(0.2, 0.6)$]. By comparing the MT mode and the HT mode, the results show that the HT mode can save more energy for the follower because the leading plate of this mode provides constructive streamwise velocity for the follower.

In collective locomotion, whether the flapping kinematics is the same or not, the follower obtains the same propulsion velocity as the leader, but consumes different energy. It indicates the propulsive efficiency of the follower is also different from that of a solitary one with the same duty. Figure 11 shows the propulsive efficiency of the follower for all orderly configurations showed in Fig. 9. For the MT mode with $DC_F = DC_L = DC$, the efficiency of the follower is smaller than the leader when $DC \leq 0.5$ or $DC = 1.0$. For $0.6 \leq DC \leq 0.9$, there are some equilibrium positions for the follower to consume more energy than a solitary plate with the same duty. For $DC_F > DC_L$, the efficiency of the follower is greater than the leader and a solitary plate with the same duty. For $DC_F < DC_L$, the efficiency of the follower is smaller than the leader. For the HT mode, the efficiency of the follower is greater than that of the leader, and is also greater than a solitary plate with the same duty (except for a few points). By comparing the MT mode and the HT mode, the results show that the HT mode can be more effective. Moreover, if there are more than one stable positions, usually the one closest to the leader is most effective. For example, for $(DC_L, DC_F) = (0.9, 1.0)$, the efficiency of the follower at the nearest stable position can improve more than twice, while that of the follower at the fifth stable position can only improve 25%.

Figure 12 shows the cost of transport (COT_F) of the follower as a function of the propulsion velocity. It is seen that, when the propulsion velocity is greater than a critical value (about five for the MT mode, about four for the HT mode), the cost of transport of the follower is smaller than that of a solitary plate with the same propulsion velocity. It indicates that collective intermittent swimming with lower duty cycle can show better energy economy in terms of the cost of transport.

IV. CONCLUSIONS

In summary, the propulsive performances of the intermittent swimming of two self-propelled flapping plates in tandem configuration are investigated numerically. It is found that, for solitary plate swimming intermittently by maintaining a bout time of unit while changing the duty cycle, the propulsion velocity and energy consumption decrease monotonically as the duty cycle DC increases, consistent

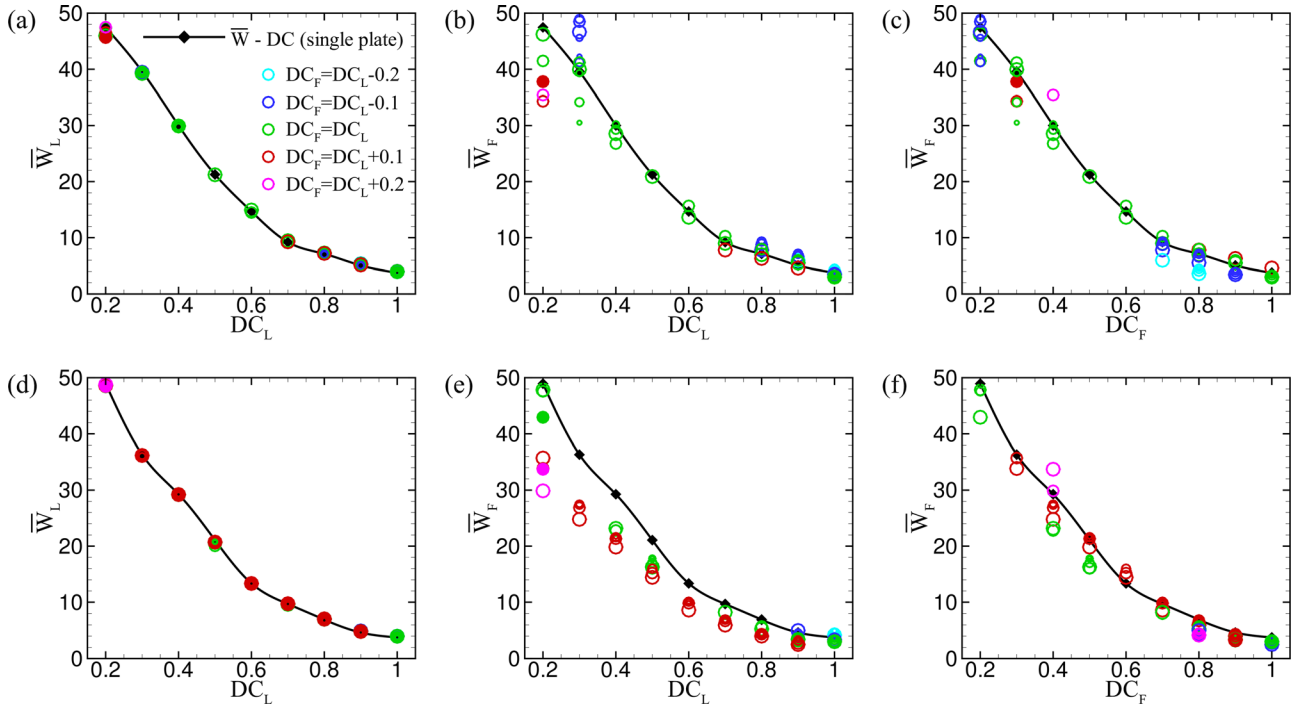


FIG. 10. [(a) and (d)] The leader's input work (\bar{W}_L) and [(b) and (e)] the follower's input work (\bar{W}_F) as a function of the duty cycle (DC_L) of the leader. [(c) and (f)] The follower's input work (\bar{W}_F) as a function of the duty cycle (DC_F) of the follower. (a)–(c) The MT mode. (d)–(f) The HT mode.

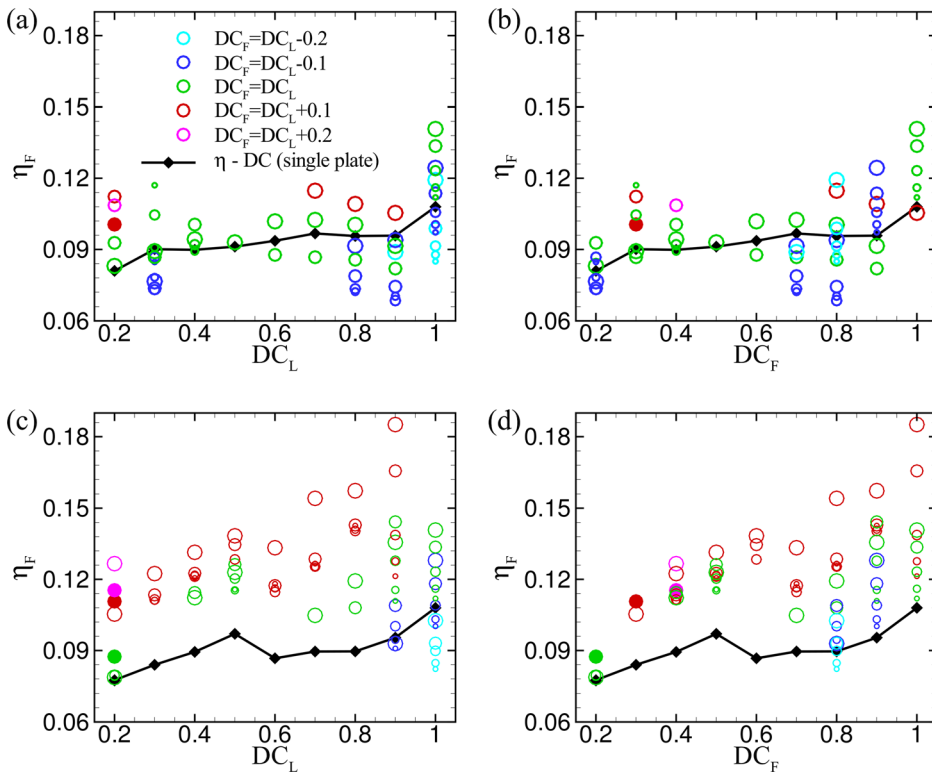


FIG. 11. The propulsive efficiency (η_F) of the follower as a function of [(a) and (c)] the duty cycle (DC_L) of the leader and [(b) and (d)] the duty cycle (DC_F) of the follower, respectively. [(a) and (b)] The MT mode. [(c) and (d)] The HT mode.

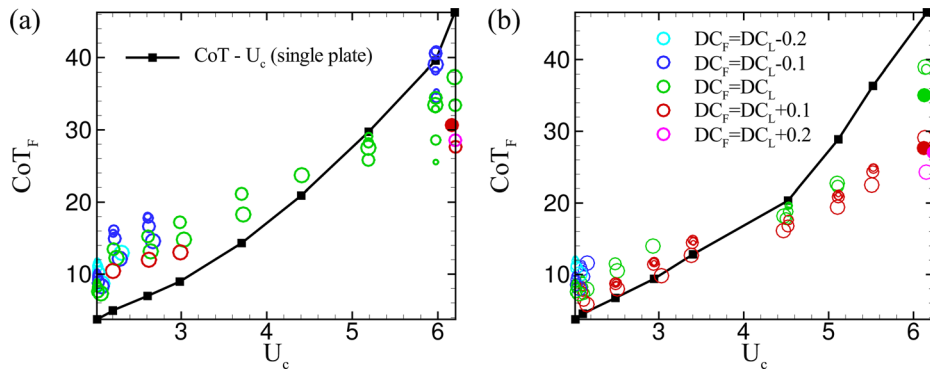


FIG. 12. The cost of transport (CoT_F) of the follower as a function of the propulsion velocity (U_c) for (a) the MT mode and (b) the HT mode, respectively.

with the prediction of the reduced-order model. No significant difference of propulsive performance between the MT-mode intermittent swimming and HT-mode intermittent swimming was found.

The wake structures for the MT-mode intermittent swimming mainly consist of two vortex streets. The upper street is mainly formed during the coast phase, while the lower street is formed during the burst phase. The wake structures for the HT-mode intermittent swimming mainly consist of three vortex streets. The two oblique streets contain strong vortex dipoles formed during the burst phase, the middle street is formed by wake vortices shed during the coast phase. Correspondingly, the time-averaged streamwise velocities of the MT-mode and HT-mode intermittent swimming are formed by two-layer structures and three-layer structures, respectively. For the MT mode, the wake in region $y \in [-A, A]$ is mainly of jet type, except for the far-field wake of $DC = 0.2$. For the HT mode, the wake in the same region is of wake type.

For two plates swimming intermittently and independently, only when their duty cycles are similar can they form a stable configuration. For the MT mode, the wake of the leader is mainly of jet type, enhancing the drag on the follower and making it harder to follow. For the HT mode, the wake of the leader is mainly of wake type, reducing the drag on the follower and making it easier to follow. No significant difference was found in the propulsive performance of intermittent swimming between leading plates in orderly configurations and solitary plates. The results of efficiency indicate that the HT mode is more economical than the MT mode for the follower. Usually, the smaller the equilibrium gap spacing is, the more efficient the follower is. The results of the cost of transport show that the follower can obtain better energy economy for higher propulsion velocity.

The present results may be helpful to further understand the combination of intermittent swimming and collective behavior of fish and may be useful for bionic design.

ACKNOWLEDGMENTS

The authors acknowledge the support of the National Natural Science Foundation of China (Grant Nos. 12102365, 11872064, and 11621202), the China Postdoctoral Science Foundation (No. 2021M692881), Guangdong Key R&D Program of 2021 Ocean Six Industrial Project (No. 2021-45), the “Construction of a Leading Innovation Team” project by the Hangzhou Municipal government,

and the Startup funding of New-joined PI of Westlake University with Grant No. 041030150118.

AUTHOR DECLARATIONS

Conflict of Interest

The authors have no conflicts to disclose.

DATA AVAILABILITY

The data that support the findings of this study are available from the corresponding author upon reasonable request.

NOMENCLATURE

A	Flapping amplitude
COT	Cost of transport for a unit mass to travel a unit distance
DC	Duty cycle of B&C swimming ($DC = 1/(1 + T_b/T_c)$)
DC_L, DC_F	Duty cycles of leading plate and following plate
Eh, EI	Structural stretching rigidity and bending rigidity
e_x	Unit vector in the x direction
F_s	Lagrangian force vector
f	Flapping frequency of the full cycle ($f = 1/T_{cyc}$)
f_b	Flapping frequency of the burst phase ($f_b = 1/(DC \cdot T_{cyc}) = f/DC$)
f	Eulerian force vector
G	Gap spacing between two plates
G_{eq}	Equilibrium gap spacing between two plates
K	Bending stiffness ($K = EI/\rho U_{ref}^2 L^3$)
L	Length of the plate
M	Mass ratio of the plate ($M = \rho_s h/\rho L$)
p	Pressure of the fluid
Re	Reynolds number ($Re = \rho U_{ref} L/\mu$)
S	Stretching stiffness ($S = Eh/\rho U_{ref}^2 L$)
s	Lagrangian coordinate along the plate
T_b, T_c	Burst and coast time in B&C swimming
T_{cyc}	Period of a complete cycle for B&C swimming
t	Time
U	Dimensionless propulsion velocity
U_c	Dimensionless mean propulsion velocity
U_{ref}	Reference velocity for nondimensionlization ($U_{ref} = Lf$)

\mathbf{u}	Velocity vector
u'	Streamwise velocity in the wake of the leader
\bar{u}'	Time-averaged streamwise velocity in the wake of the leader
u_i	Propulsion velocity of the i th plate
W	Dimensionless input work
\bar{W}	Dimensionless mean input work
\mathbf{X}	Position vector for plate
\mathbf{x}	Position vector for flow fluid
y_{head}, y_{tail}	Lateral position of the leading edge and the trailing edge of the plate
η	Propulsive efficiency
λ	The wavelength of the leading plate ($\lambda = U_c(DC_L)T_{cyc}$)
μ	Dynamic viscosity of the fluid
ρ	Density of the fluid
$\rho_s h$	Structural linear mass density

APPENDIX A: THE NUMERICAL METHOD DETAILS

In the present work, the kinetics of the fluid is governed by the discrete lattice Boltzmann equation (LBE) of a single relaxation time model,^{51,63,64} and the multi-block lattice Boltzmann technique⁶⁵ has been incorporated. The LBE with the Bhatnagar–Gross–Krook (BGK) model⁶⁶ is

$$f_i(\mathbf{x} + \mathbf{e}_i \Delta t, t + \Delta t) - f_i(\mathbf{x}, t) = -\frac{1}{\tau} [f_i(\mathbf{x}, t) - f_i^{eq}(\mathbf{x}, t)] + \Delta t F_i, \quad i = 0, \dots, 8, \tag{A1}$$

where f_i is the i th particle distribution function with discrete speed \mathbf{e}_i at position \mathbf{x} and time t . Δx and Δt are the grid spacing and time step, respectively. $\tau = (\nu/c_s^2 \Delta t + 0.5)$ is the nondimensional relaxation time associated with kinematic viscosity ν , where $c_s = (\Delta x/\Delta t)/\sqrt{3}$ is the lattice sound speed. The equilibrium distribution function f_i^{eq} and the forcing term F_i are defined as^{63,67}

$$f_i^{eq} = \omega_i \rho \left[1 + \frac{\mathbf{e}_i \cdot \mathbf{u}}{c_s^2} + \frac{\mathbf{u} \mathbf{u} : (\mathbf{e}_i \mathbf{e}_i - c_s^2 \mathbf{I})}{2c_s^4} \right], \quad i = 0, \dots, 8, \tag{A2}$$

$$F_i = \left(1 - \frac{1}{2\tau} \right) \omega_i \left[\frac{\mathbf{e}_i - \mathbf{u}}{c_s^2} + \frac{\mathbf{e}_i \cdot \mathbf{u}}{c_s^4} \mathbf{e}_i \right] \cdot \mathbf{f}, \quad i = 0, \dots, 8, \tag{A3}$$

where ω_i is the weighting factor depending on the lattice model ($\omega_0 = 4/9, \omega_1 = \omega_2 = \omega_3 = \omega_4 = 1/9, \omega_5 = \omega_6 = \omega_7 = \omega_8 = 1/36$). ρ, \mathbf{u} , and \mathbf{f} are the macroscopic fluid density, velocity, and body force, respectively, as defined in Eq. (3).

The mass density and velocity can be obtained by the distribution functions

$$\rho = \sum_i f_i, \tag{A4}$$

$$\rho \mathbf{u} = \sum_i \mathbf{e}_i f_i + \frac{1}{2} \mathbf{f} \Delta t. \tag{A5}$$

Equation (5) for the plate is discretized by a finite element method. The motion of the plate is handled by the corotational scheme.⁵³ In this scheme, a local coordinate system is envisioned to

move with each discrete element, and the element behaves linearly relative to the moving coordinate system. Consequently, the nonlinearity of the problem goes to the coordinate transformation.

In the IB method, the Lagrangian interaction force F_s [used in Eq. (5)] can be calculated by the feedback law⁵⁴

$$F_s(s, t) = \alpha \int_0^t [V_f(s, t') - V_s(s, t')] dt' + \beta [V_f(s, t) - V_s(s, t)], \tag{A6}$$

where α and β are free parameters to enforce the no-slip condition, which are selected based on Hua *et al.*⁵⁵ V_f is the fluid velocity at the position of the body, which is obtained by interpolation and given by

$$V_f(s, t) = \int_{\Gamma} \mathbf{u}(\mathbf{x}, t) \delta(\mathbf{x} - \mathbf{X}(s, t)) d\mathbf{x}, \tag{A7}$$

where the plate boundary Γ is denoted by the Lagrangian coordinates $\mathbf{X}(s, t)$. The Eulerian body force \mathbf{f} [used in Eq. (3)] can be calculated as follows:

$$\mathbf{f}(\mathbf{x}, t) = - \int_{\Gamma} F_s(s, t) \delta(\mathbf{x} - \mathbf{X}(s, t)) ds. \tag{A8}$$

In the present work, a four-point regularized δ function⁵⁴ is used.

APPENDIX B: SIMPLIFIED DYNAMICAL MODEL

Here, we consider the swimming of solitary plate. According to Newton’s second law,

$$m \dot{u} = T - D, \tag{B1}$$

where m is the mass of the plate plus some added mass of water. T and D are the thrust and drag on the plate, respectively. According to the inviscid flow theory^{9,69} and the scaling law for thrust coefficient proposed by Floryan *et al.*,⁴⁰ the thrust T behaves like v^2 , i.e.,

$$T = \frac{1}{2} \rho L c_t v^2 = c v^2, \tag{B2}$$

where c_t is the (constant) thrust coefficient, ρ the fluid density, and L the length of the plate. The drag of a given rigid body depends on the square of the propulsion velocity,³⁴ i.e.,

$$D = \frac{1}{2} \rho L c_d u^2 = d u^2, \tag{B3}$$

where c_d is (constant) drag coefficient. According to the experimental data for real fish,^{36,68} the drag of fish when swimming is increased over the value for a rigid body by a factor (α) of approximately 3, so during the burst stage, $D = \alpha d u^2$.

It is noted that the above modeling strategy ($T \sim v^2, D \sim u^2$) has been successfully applied to many studies, such as the prediction of energy economy of intermittent locomotion,^{27,34} the continuous locomotion of two self-propelled foils/plates,^{18,21} and good predictions have been obtained.

Integrating Eq. (B1) in the burst period and coast period (the MT mode for example), we can obtain

$$m(U_f - U_i) = \int_{T_b} (cv^2 - \alpha du^2) ds, \tag{B4}$$

$$m(U_i - U_f) = \int_{T_c} (-du^2) ds, \tag{B5}$$

where U_i and U_f denote the initial velocity and final velocity of the burst phase, respectively. Adding Eqs. (B4) and (B5) yields

$$\int_{T_b} cv^2 dt = \int_{T_b} \alpha du^2 dt + \int_{T_c} du^2 dt. \tag{B6}$$

Substituting Eq. (1) into Eq. (B6), Eq. (B6) can be rewritten as follows:

$$\frac{2c}{d} (\pi A)^2 = T_b \left(\int_{T_b} \alpha u^2 dt + \int_{T_c} u^2 dt \right), \tag{B7}$$

where the left-hand side of Eq. (B7) is constant.

To conveniently predict the relation between the propulsion velocity and the duty cycle, we ignore the change of propulsion velocity with time and replace u by U_c , and set $\alpha = 3$; then, Eq. (B7) can be reduced to

$$\frac{2c}{d} (\pi A)^2 = U_c^2 T_{cyc} (DC + 2DC^2). \tag{B8}$$

So, the relation between the propulsion velocity and the duty cycle is

$$U_c = \beta \frac{1}{\sqrt{DC + 2DC^2}}, \tag{B9}$$

where $\beta = \left(\sqrt{\frac{2c}{d} \frac{\pi A}{T_{cyc}}} \right)$ is a constant coefficient in the present work, because T_{cyc} is fixed. The energy required per cycle is

$$\bar{W} = \int_{T_b} \frac{Tu}{\eta} dt = \int_{T_b} \frac{cv^2 u}{\eta} dt. \tag{B10}$$

At high velocities, the efficiency η can be approximately constant.²⁷ By adopting $u = U_c$, we can obtain

$$\bar{W} = \frac{U_c}{\eta} \frac{2c(\pi A)^2}{T_b} = \gamma \frac{1}{DC\sqrt{DC + 2DC^2}}, \tag{B11}$$

where $\gamma = \left(\frac{1}{\eta} \sqrt{\frac{8c^3}{d} \frac{(\pi A)^3}{T_{cyc}}} \right)$ is a constant coefficient.

REFERENCES

¹E. Shaw, "Schooling fishes: The school, a truly egalitarian form of organization in which all members of the group are alike in influence, offers substantial benefits to its participants," *Am. Sci.* **66**, 166–175 (1978).
²D. Weihs, "Hydromechanics of fish schooling," *Nature* **241**, 290–291 (1973).
³C. M. Breder, "Fish schools as operational structures," *Fish. Bull.* **74**, 471–502 (1976).
⁴V. V. Belyayev and G. V. Zuyev, "Hydrodynamic hypothesis of school formation in fishes," *J. Ichthyol.* **9**, 578–584 (1969).
⁵P. A. Fields, "Decreased swimming effort in groups of pacific mackerel (*Scomber-japonicus*)," *Am. Zool.* **30**, A134–A134 (1990).
⁶J. Herskin and J. F. Steffensen, "Energy savings in sea bass swimming in a school: Measurements of tail beat frequency and oxygen consumption at different swimming speeds," *J. Fish Biol.* **53**, 366–376 (1998).

⁷B. L. Partridge, "The structure and function of fish schools," *Am. Sci.* **246**, 114–123 (1982).
⁸D. S. Pavlov and A. O. Kasumyan, "Patterns and mechanisms of schooling behavior in fish: A review," *J. Ichthyol.* **40**, S163–S231 (2000).
⁹M. J. Lighthill, *Mathematical Biofluid Dynamics* (SIAM, Philadelphia, 1975).
¹⁰B. L. Partridge and T. J. Pitcher, "Evidence against a hydrodynamic function for fish schools," *Nature* **279**, 418–419 (1979).
¹¹T. M. Broering and Y. S. Lian, "The effect of phase angle and wing spacing on tandem flapping wings," *Acta Mech. Sin.* **28**, 1557–1571 (2012).
¹²B. M. Boschitsch, P. A. Dewey, and A. J. Smits, "Propulsive performance of unsteady tandem hydrofoils in an in-line configuration," *Phys. Fluids* **26**, 051901 (2014).
¹³G. D. Xu and W. Xu, "Energy extraction of two flapping foils with tandem configurations and vortex interactions," *Eng. Anal. Boundary Elem.* **82**, 202–209 (2017).
¹⁴B. Ribeiro, Y. Su, Q. Guillaumin, K. S. Breuer, and J. A. Franck, "Wake-foil interactions and energy harvesting efficiency in tandem oscillating foils," *Phys. Rev. Fluids* **6**, 074703 (2021).
¹⁵X. J. Zhu, G. W. He, and X. Zhang, "Flow-mediated interactions between two self-propelled flapping filaments in tandem configuration," *Phys. Rev. Lett.* **113**, 238105 (2014).
¹⁶S. Ramanarivo, F. Fang, A. Oza, J. Zhang, and L. Ristroph, "Flow interactions lead to orderly formations of flapping wings in forward flight," *Phys. Rev. Fluids* **1**, 071201 (2016).
¹⁷Z.-R. Peng, H. B. Huang, and X.-Y. Lu, "Collective locomotion of two closely spaced self-propelled flapping plates," *J. Fluid Mech.* **849**, 1068–1095 (2018).
¹⁸J. W. Newbolt, J. Zhang, and L. Ristroph, "Flow interactions between uncoordinated flapping swimmers give rise to group cohesion," *Proc. Natl. Acad. Sci. U. S. A.* **116**, 2419–2424 (2019).
¹⁹Y. Pan and H. B. Dong, "Computational analysis of hydrodynamic interactions in a high-density fish school," *Phys. Fluids* **32**, 121901 (2020).
²⁰H. Y. Yu, X.-Y. Lu, and H. B. Huang, "Collective locomotion of two uncoordinated undulatory self-propelled foils," *Phys. Fluids* **33**, 011904 (2021).
²¹L. L. Kang, Z. R. Peng, H. B. Huang, X.-Y. Lu, and W. C. Cui, "Active external control effect on the collective locomotion of two tandem self-propelled flapping plates," *Phys. Fluids* **33**, 101901 (2021).
²²X. H. Li, J. Y. Gu, Z. Su, and Z. Q. Yao, "Hydrodynamic analysis of fish schools arranged in the vertical plane," *Phys. Fluids* **33**, 121905 (2021).
²³D. L. Kramer and R. L. McLaughlin, "The behavioral ecology of intermittent locomotion," *Am. Zool.* **42**, 137–153 (2001).
²⁴D. Weihs, "Energetic significance of changes in swimming modes during growth of larval anchovy, *Engraulis mordax*," *Fish. Bull.* **77**, 597–604 (1980).
²⁵F. E. Fish, J. F. Fegely, and C. J. Xanthopoulos, "Burst-and-coast swimming in schooling fish (*Notemigonus crysoleucas*) with implications for energy economy," *Comp. Biochem. Physiol. Part A* **100**, 633–637 (1991).
²⁶G. Wu, Y. Yang, and L. Zeng, "Kinematics, hydrodynamics and energetic advantages of burst-and-coast swimming of koi carps (*Cyprinus carpio koi*)," *J. Exp. Biol.* **210**, 2181 (2007).
²⁷J. J. Videler and D. Weihs, "Energetic advantages of burst-and-coast swimming of fish at high speeds," *J. Exp. Biol.* **97**, 169–178 (1982).
²⁸R. W. Blake, "Functional design and burst-and-coast swimming in fishes," *Can. J. Zool.* **61**, 2491–2494 (1983).
²⁹U. Müller, E. J. Stamhuis, and J. J. Videler, "Hydrodynamics of unsteady fish swimming and the effects of body size: Comparing the flow fields of fish larvae and adults," *J. Exp. Biol.* **203**, 193–206 (2000).
³⁰M. J. McHenry, "The mechanical scaling of coasting in zebrafish (*Danio rerio*)," *J. Exp. Biol.* **208**, 2289–2301 (2005).
³¹I. Ashraf, H. Bradshaw, T. T. Ha, J. Halloy, R. Godoy-Diana, and B. Thiria, "Simple phalanx pattern leads to energy saving in cohesive fish schooling," *Proc. Natl. Acad. Sci. U. S. A.* **114**, 9599–9604 (2017).
³²G. Li, I. Ashraf, B. Franois, D. Kolomenskiy, F. Lechenault, R. Godoy-Diana, and B. Thiria, "Burst-and-coast swimmers optimize gait by adapting unique intrinsic cycle," *Commun. Biol.* **4**, 40 (2021).
³³T. Noda, K. Fujioka, H. Fukuda, H. Mitamura, K. Ichikawa, and N. Arai, "The influence of body size on the intermittent locomotion of a pelagic schooling fish," *Proc. R. Soc. B* **283**, 20153019 (2016).

- ³⁴D. Weihs, "Energetic advantages of burst swimming of fish," *J. Theor. Biol.* **48**, 215–229 (1974).
- ³⁵J. J. Videler, "Swimming movements, body structure and propulsion in cod (*Gadus morhua*)," in *Vertebrate Locomotion*, edited by M. H. Day (Academic Press, London, 1981), pp. 1–27.
- ³⁶M. J. Lighthill, "Large-amplitude elongated-body theory of fish locomotion," *Proc. R. Soc. London, Ser. B* **179**, 125–138 (1971).
- ³⁷E. Akoz and K. W. Moored, "Unsteady propulsion by an intermittent swimming gait," *J. Fluid Mech.* **834**, 149–172 (2018).
- ³⁸E. Akoz, A. Mivehchi, and K. W. Moored, "Intermittent unsteady propulsion with a combined heaving and pitching foil," *Phys. Rev. Fluids* **6**, 043101 (2021).
- ³⁹M. H. Chung, "On burst-and-coast swimming performance in fish-like locomotion," *Bioinspiration Biomimetics* **4**, 036001 (2009).
- ⁴⁰D. Floryan, T. V. Buren, and A. J. Smits, "Forces and energetics of intermittent swimming," *Acta Mech. Sin.* **33**, 725 (2017).
- ⁴¹J. Ryu and H. J. Sung, "Intermittent locomotion of a self-propelled plate," *Phys. Fluids* **31**, 111902 (2019).
- ⁴²L. Dai, G. W. He, Z. Xiang, and Z. Xing, "Intermittent locomotion of a fish-like swimmer driven by passive elastic mechanism," *Bioinspiration Biomimetics* **13**, 056011 (2018).
- ⁴³K. Liu, H. B. Huang, and X.-Y. Lu, "Hydrodynamic benefits of intermittent locomotion of a self-propelled flapping plate," *Phys. Rev. E* **102**, 053106 (2020).
- ⁴⁴S. Gupta, N. Thekkethil, A. Agrawal, K. Hourigan, M. C. Thompson, and A. Sharma, "Body-caudal fin fish-inspired self-propulsion study on burst-and-coast and continuous swimming of a hydrofoil model," *Phys. Fluids* **33**, 091905 (2021).
- ⁴⁵I. Ashraf, S. V. Wassenbergh, and S. Verma, "Burst-and-coast swimming is not always energetically beneficial in fish (*Hemigrammus bleheri*)," *Bioinspiration Biomimetics* **16**, 016002 (2021).
- ⁴⁶Q. Bone, J. Kiceniuk, and D. R. Jones, "On the role of the different fibre types in fish myotome at intermediate speeds," *Fish. Bull.* **76**, 691–699 (1978).
- ⁴⁷I. Asharf, "Interactions in collective fish swimming," Ph.D. thesis (Université Sorbonne Paris Cité, 2018).
- ⁴⁸J. C. Liao, D. N. Beal, G. V. Lauder, and M. S. Triantafyllou, "Fish exploiting vortices decrease muscle activity," *Science* **302**, 1566–1569 (2003).
- ⁴⁹J. Hunter and J. Zweifel, "Swimming speed, tail beat frequency, tail beat amplitude, and size in jack mackerel, *Trachurus symmetricus*, and other fishes," *Fish. Bull.* **69**, 253–265 (1971).
- ⁵⁰B. S. H. Connell and D. K. P. Yue, "Flapping dynamics of a flag in a uniform stream," *J. Fluid Mech.* **581**, 33–67 (2007).
- ⁵¹S. Y. Chen and G. D. Doolen, "Lattice Boltzmann method for fluid flows," *Annu. Rev. Fluid Mech.* **30**, 329–329 (1998).
- ⁵²S. Succi, *The Lattice Boltzmann Equation for Fluid Dynamics and Beyond* (Oxford University Press, 2001).
- ⁵³J. Doyle and E. Desantiago, "Nonlinear analysis of thin-walled structures: Statics, dynamics, and stability. Mechanical engineering series," *Appl. Mech. Rev.* **55**, B92 (2002).
- ⁵⁴C. S. Peskin, "The immersed boundary method," *Acta Numer.* **11**, 479–517 (2002).
- ⁵⁵R.-N. Hua, L. D. Zhu, and X.-Y. Lu, "Locomotion of a flapping flexible plate," *Phys. Fluids* **25**, 121901 (2013).
- ⁵⁶R.-N. Hua, L. Zhu, and X.-Y. Lu, "Dynamics of fluid flow over a circular flexible plate," *J. Fluid Mech.* **759**, 56–72 (2014).
- ⁵⁷C. Tang, N. S. Liu, and X.-Y. Lu, "Dynamics of an inverted flexible plate in a uniform flow," *Phys. Fluids* **27**, 073601 (2015).
- ⁵⁸Z.-R. Peng, H. B. Huang, and X.-Y. Lu, "Hydrodynamic schooling of multiple self-propelled flapping plates," *J. Fluid Mech.* **853**, 587–600 (2018).
- ⁵⁹A. De Rosis, G. Falcucci, S. Ubertini, and F. Ubertini, "A coupled lattice Boltzmann-finite element approach for two-dimensional fluid-structure interaction," *Comput. Fluids* **86**, 558–568 (2013).
- ⁶⁰A. De Rosis, S. Ubertini, and F. Ubertini, "A partitioned approach for two-dimensional fluid-structure interaction problems by a coupled lattice Boltzmann-finite element method with immersed boundary," *J. Fluids Struct.* **45**, 202–215 (2014).
- ⁶¹A. De Rosis, G. Falcucci, S. Ubertini, and F. Ubertini, "Aeroelastic study of flexible flapping wings by a coupled lattice Boltzmann-finite element approach with immersed boundary method," *J. Fluids Struct.* **49**, 516–533 (2014).
- ⁶²B. Kim, S. G. Park, W. Huang, and H. J. Sung, "Self-propelled heaving and pitching flexible fin in a quiescent flow," *Int. J. Heat Fluid Flow* **62**, 273–281 (2016).
- ⁶³Z. L. Guo, C. G. Zheng, and B. C. Shi, "Discrete lattice effects on forcing terms in the lattice Boltzmann method," *Phys. Rev. E* **65**, 046308 (2002).
- ⁶⁴C. K. Aidun and J. R. Clausen, "Lattice-Boltzmann method for complex flows," *Annu. Rev. Fluid Mech.* **42**, 439–472 (2010).
- ⁶⁵D. Yu, R. Mei, and W. Shyy, "A multi-block lattice Boltzmann method for viscous fluid flows," *Int. J. Numer. Methods Fluids* **39**, 99–120 (2002).
- ⁶⁶P. Bhatnagar, E. Gross, and M. Krook, "A model for collision processes in gases. I. Small amplitude processes in charged and neutral one-component systems," *Phys. Rev.* **94**, 511–525 (1954).
- ⁶⁷Y. Cheng and J. Li, "Introducing unsteady non-uniform source terms into the lattice Boltzmann model," *Int. J. Numer. Methods Fluids* **56**, 629–641 (2008).
- ⁶⁸P. W. Webb, "The swimming energetics of trout," *J. Exp. Biol.* **55**, 521–540 (1971).
- ⁶⁹Y. T. Wu, "Swimming of a waving plate," *J. Fluid Mech.* **10**, 321–344 (1961).